CrystEngComm

Accepted Manuscript

This is an *Accepted Manuscript*, which has been through the Royal Society of Chemistry peer review process and has been accepted for publication.

Accepted Manuscripts are published online shortly after acceptance, before technical editing, formatting and proof reading. Using this free service, authors can make their results available to the community, in citable form, before we publish the edited article. We will replace this *Accepted Manuscript* with the edited and formatted *Advance Article* as soon as it is available.

You can find more information about *Accepted Manuscripts* in the **Information for Authors**.

Please note that technical editing may introduce minor changes to the text and/or graphics, which may alter content. The journal's standard **Terms & Conditions** and the **Ethical guidelines** still apply. In no event shall the Royal Society of Chemistry be held responsible for any errors or omissions in this *Accepted Manuscript* or any consequences arising from the use of any information it contains.

Crystallographic Fusion Behavior and Interface Evolution of

Mono-Layer BaTiO$_3$ Nanocube Arrangement

Qiang Ma* and Kazumi Kato

*National Institute of Advanced Industrial Science and Technology (AIST),
2266-98 Anagahora, Shimoshidami, Moriyama, Nagoya, 463-8560, Japan*

A crystallographic fusion behavior between $BaTiO_3$ nanocubes with variable sintering temperatures and geometries was investigated by precise analysis using high resolution transmission electron microscopy (HRTEM). The fine orderly microstructure of nanocubes arrangement remained even after high temperature sintering process ($\sim$900°C), where the face-to-face connection with simple cubic symmetry was stable. By using FFT filtered HRTEM images, we revealed the atom-scale crystalline coherence of neighboring $BaTiO_3$ nanocubes in the connection. In the case of the small angle relation of nanocubes, the initial ambient interface changed into robust structure at one critical sintering temperature, and the finally lattice defects evolved in the interface region. The lattice fringes in different nanocubes grew and connected via an atom-by-atom epitaxial attachment mechanism, and a well semi-coherent fusion region was formed around 850°C. The amount of defects has a close relationship with the sintering temperature. Combined with the results of our previous research, the evolved nano-architecture consisting of the ordered nanocubes and interfaces plays a key role in the enhancement of dielectric properties.

1. Introduction

Barium titanate ($BaTiO_3$) nanocrystals have fascinated scientists and engineers' great attention because of their potential applications on varies industrial devices, such as ferroelectric memory devices, multilayer ceramic capacitors, optical modulators, IR detectors, etc.[1-6] Especially, $BaTiO_3$ nanocrystals with cubic shape possess unique physical and chemical properties, derived from their peculiar symmetries and specific superstructures.[7-14] In the last decade, the focus of the research on $BaTiO_3$ nanocrystals is gradually shifting to their self-assembly and excellent dielectric property. To date, $BaTiO_3$ nanocrystals were usually used as ceramic fillers of nano-composited films to improve the dielectric constant.[15-18] Recently, it was found that metal-insulator-metal (MIM) capacitors being consisted of the nanocube assemblies and Pt electrodes exhibited the enhanced dielectric properties such as dielectric constant of 4000 and loss of 0.07.[10, 11] Moreover, the dielectric properties were influenced by the sintering temperature of the MIM capacitors. Compared with the bulk crystal of $BaTiO_3$ and mono-dispersed $BaTiO_3$ nanocrystals, the distinguishable interface conditions among neighboring nanocubes in assemblies was considered to play a key crucial role on the improved dielectric properties.

However, the mechanism of $BaTiO_3$ nanocubes assembles on the high dielectric

properties is ambiguous. The lack of consensus on the dielectric properties of $BaTiO_3$ nanocubes is mainly due to the lack of detailed study and direct evidence on their interaction behavior during sintering process. The assembly of nanocubes will result in a large interfacial area, which is prone to high defect concentrations. It is well known that the functionalities and performances of nanomaterials are strongly influenced by their structural defects. The study on the structural defects in nanocrystal super-lattice has been carried on by several groups using high-resolution TEM.[19-22] Markovich et.al pointed out that the defect density at the grain boundaries of MgO nanosheet could cause an increased dielectric constant, [19] but the mechanism was still unclear. To push the advance of the investigation of this mechanism, the interaction behavior of neighbored $BaTiO_3$ nanocubes is a key point to be precisely analyzed. A kinetic Monte Carlo modeling has been employed to study the sintering behavior of nanocrystal layer. [23] The sintering process involves a non-equilibrium dynamics for transporting of nanomaterials, which can affect the layer morphology in large area. To date, based on our best knowledge, no report focused on the temperature-dependence of interaction in $BaTiO_3$ nanocubes arrangement and the dislocations behavior in the interface between nanocubes. In order to develop the dielectric devices based on BT nanocubes, it is necessary to investigate the defect engineering of the interface between $BaTiO_3$

nanocubes undergoing the high-temperature sintering process.

In this paper, $BaTiO_3$ nanocubes with {100} face-to-face structure were fabricated by a simple drop-casting process. Here, to shed light on the relationship between the interface region structure of $BaTiO_3$ nanocube arrangements and the sintering temperature, we have carried out a precise study on the sintering behavior of the arrangement of $BaTiO_3$ nanocubes by employing the HRTEM. In our scheme, the study elucidated the interface of $BaTiO_3$ nanocubes arrangement with the increase on the sintering temperature and the types of defects in the interface region between $BaTiO_3$ nanocubes.

2. Experimental

$BaTiO_3$ nanocubes were synthesized by the hydrothermal method, which has been published in previous articles.[9] $BaTiO_3$ nanocubes were dispersed into mesitylene solution and dropped on silicon substrate by Gilson pipettes. After drying at room temperature, the samples were sintered in a furnace at different temperatures for 1 hour under oxygen gas atmosphere. To observe the interface condition of $BaTiO_3$ nanocubes arrangements, the samples were transferred from silicon substrate to TEM mesh by the following simple process. At first, the sintered silicon substrates with $BaTiO_3$ nanocubes were immersed into ethanol solution for several hours in a glass bottle. Then, the bottle

was put in an ultrasonic device to peel the $BaTiO_3$ nanocubes arrangement from silicon substrate. Finally, the ethanol solution with a quite amount of $BaTiO_3$ nanocubes arrangement pieces was dropped on the TEM grids and Si substrates by Gilson pipettes.

The $BaTiO_3$ nanocubes were characterized by X-ray diffractometer (XRD, Rigaku RINT-2100V). The morphology of the prepared $BaTiO_3$ nanocubes arrangement was investigated by using a field emission scanning electron microscope (FESEM, JEOL JSM-6335FM) and a transmission electron microscopy (TEM; Model JEM-2010F, with an accelerating voltage of 200 kV).

3. Results and discussion

Fig.1 shows the FE-SEM images of $BaTiO_3$ nanocubes arrangements with and without sintering process. The sintering temperatures were 800^oC, 850^oC and 900^oC, respectively. The $BaTiO_3$ nanocubes had {100} face-to-face arrangement within a range of several hundred nanometers. The self-arrangement of nanoparticles is a natural and spontaneous process. The self-assemble driving force is initially associated with the capillary force during evaporation of the solvent.   Thereafter, the force derives from van der Waals force, hydrogen bonding, hydrophilic/hydrophobic, electrostatic interaction, or metal−ligand coordination networks, etc.[24, 25] In this work, the van der Waals of the molecular of oleic acid played a pivotal role in the mono-layer

arrangement of nanocubes. As shown in Fig. 1 (c) and (d), the kind of arrangement

structure could be retained even after the heat treatment of $850^{\circ}C$ or $900^{\circ}C$ and

transferred into a more compact connected structure. This result indicates that the

$BaTiO_3$ nanocubes possesses a better thermal stability under high-temperature sintering

process, compared with another kind of traditional ceramic nanoparticles possessing

irregular shapes.[15-17, 26, 27] The XRD result in the inset of Fig. 1 (a) provides evidence for

the perovskite structure of $BaTiO_3$ nanocubes with a high orientation degree.

In the interface region of $BaTiO_3$ nanocubes without any sintering treatment,

amorphous phase were present and this was highlighted by a red dotted-line block in the

Fig. 2. High resolution TEM image (HRTEM) showed that an obvious amorphous layer

bridged the crystallized cube. The characteristic phenomenon revealed the amorphous

layer was derived from the oleic acid molecules, which absorbed on the surfaces of the

nanocubes. The thickness of the layer is 1.2±0.1nm, which is smaller than the length of

an oleic acid molecule (*ca*. 2nm). The result indicates that a certain tilt angle or bending

of the elastic long chain of oleic acid molecule might be present. In comparison, the

nanocubes arrangement sintered at high temperature (Fig. 4-7) for 1 hour showed

crystallite structure and no amorphous phase. This meant that the initial ambient

interface changed into a robust structure at the critical sintering temperatures. Moreover,

the HRTEM image and the corresponding FFT pattern (inset of Fig. 2) supplied the evidence for the single crystal phase of BaTiO$_3$ nanocubes.

Fig. 3 shows the TEM images of the arrangement of BaTiO$_3$ nanocubes, which was sintered for 1hour under oxygen gas atmosphere at different high temperatures. It was worth noting that the cubic shape of the BaTiO$_3$ nanocubes still exist even the temperature of sintering process reached 900°C. The observable of BaTiO$_3$ nanocubes arrays in Fig. 3 (a), (b) and (c) showed their structural stability under high temperature treatment. We employed a long-time ultrasonic method to peel off the nanocubes arrangement from the substrate. So, the BaTiO$_3$ nanocubes arrays were also stable under a strong ultrasonic induced force. Fig. 3 (d) showed the images of nanocubes arrangement after 950°C sintering process. The BaTiO$_3$ nanocubes merged together and the cubic structure became blurred. The results indicates that the limit working temperature of BaTiO$_3$ nanocube based devices can reach approximately 900°C.

HRTEM images can provide valuable information regarding the interface structure and orientation of the BaTiO$_3$ nanocubes arrangement. For better visibility and discussion, all of HRTEM images shown in the main text have been Fourier filtered. Fig. 4 shows the HRTEM images of the arrangement of BaTiO$_3$ nanocubes, which was sintered at 800°C for 1hour under oxygen gas atmosphere. Fig. 4 (a) revealed that the

surfaces of the nanocubes were clean, and without any sheathed amorphous phase. The

FFT filtered image of Fig. 4 (b) displayed that edge dislocations existed in the interface

region of the $BaTiO_3$ nanocubes arrangement and resulted in the violation of

translational symmetry along a straight line. The dislocations were originated to

accommodate the misalignment of neighboring nanocubes. The Fig. 4 (b) provided the

detailed information for the misalignment of crystal fringes of neighboring $BaTiO_3$

nanocubes. It was considered that the thermal expansion and epitaxial connection of

neighboring nanocubes during the sintering process resulted in the formation of the

misalignment and the edge dislocation.[28] The edge dislocation line is normal to [100]

projection of $BaTiO_3$ lattice. The burgers vector (b) of the edge dislocation could be

obtained by drawing a Burgers circuit around the dislocation, [29, 30] marked by white

dotted-line and red arrow in the inset of Fig. 4 (b). The core region of the edge

dislocations possessed dangling bonds, and was usually associated with notably strain

fields and local electronic states.[31, 32] Consequently, Cottrell atmospheres could be

produced around the dislocation. As displayed by Fig. 4-7, the amount of the edge

dislocation was dependent on the sintering temperature. In addition, one interesting

feature observed in Fig. 4 (b) is the moiré pattern, marked by the white line. Moiré

pattern is an interference pattern of two overlaid gratings with a certain angle or with

different periodicities.[14, 21] In this work, the moiré pattern were generated through the partial superposition of the {100} lattice fringes with a small angle. The large amount of lattice defects could form some special transmission channels for electrons between $BaTiO_3$ nanocubes, and influence the dielectric property.

Lattice defects were rarely observed in the inner layer of nanocubes arrangement and more continuous lattice fringes could be observed after sintering under $850^{\circ}C$ and $900^{\circ}C$, as demonstrated in Fig. 5 and 6. This phenomenon can be attributed to the relative higher sintering temperature environment. The dynamically accommodated lattice dislocations inside the interface region of nanocube arrangement could be removed by thermal diffusion. This demonstrated the metastable nature of these lattice defects. Detailed observation of Fig. 5 (b) and 6 (b) revealed that most of {100} lattice fringes of the neighboring $BaTiO_3$ nanocubes joined together at the atomic level. This result indicated that the lattice fringes in different nanocubes grew and connected via an atom-by-atom epitaxial attachment mechanism at the relative high sintering temperatures. This attachment process played a positive role in improving the dielectric properties of nanocubes arrangement. Own to the local strain fields, dark region emerged in some place of the connecting portion of the nanocube arrangement.[33] Several edge dislocations could be observed near the fusion region to relieve the

interfacial strain. It was considered that the slightly mutual rotation or misfit between

neighboring nanocubes resulted in the formation of lattice strain after sintering.

Fig. 7 showed the HRTEM images of nanocubes arrangement after 950°C sintering

process. As displayed by Fig. 7 (a), the cubic structure and the interface between

nanocubes became blurred. The crystal fringes of the neighbored nanocubes were not

linear sharp but the form of ripples (marked by white curves in Fig. 7 (b)). The distorted

crystalline structure was related with stress release during the high-temperature sintering

process. At the edge section of BaTiO$_3$ nanocube arrangement, the stacking sequence of

crystalline structure was disrupted by the presence of line defect (marked by white line).

Fig. 7 (c) displayed the FFT filtered image, which was obtained by using only one set of

[100] spots of FFT pattern. The images showed a series of curved lattice fringes, which

was same as those in Fig. 7 (b) and marked by red dotted-line square. These results

indicated that the thermal stress mainly affected the crystalline structure of nanocubes

arrangement from the [100] crystal orientation. In addition, we did not observe the

threading dislocations. This kind of defects will create non-radiative recombination

centers and deteriorate the performance of electro-optical devices.[34]

Planar defects (small angle grain boundary) were identified in Fig. 8, where the (100)

planes between neighboring BaTiO$_3$ nanocubes were tilted. As well known, grain

boundaries form where the crystallographic direction of the lattice abruptly changes. It

could be observed that the orientations of nanocubes in Fig. 8 (a), and (c) were rotated

with respect to neighboring nanocubes for a small angle. During the high temperature

sintering process, the cube-to-cube tilt epitaxial attachment in the arrangements caused

the formation of the small angle grain boundary. The reciprocal lattice spots in FFT

patterns, corresponding to the same crystal faces, were not overlap and splitting (marked

by red arrows). This result indicated the tilt attachment of nanocubes. The inverse FFT

image in Fig. 8 (b) provided the clear view for small angle grain boundary. The tilt

angles of {100} crystal planes in neighboring $BaTiO_3$ nanocubes were estimated to be

less than 10°. The existence of the low angle grain boundary can result in dislocations at

the interface region of nanocrystals.[35] The HRTEM image of Fig. 8 (d) revealed that an

array of dislocations were along the small angle grain boundary and surrounded by

regions of perfect crystal, separately. The dislocations belonged to pure edge dislocation

with a Burgers vector of type <100>. The burgers vector of the dislocation could be

defined to be 1/2 <100> by drawing a Burgers circuit around the dislocation (showed in

inset of Fig. 8 (d)). The energy of the edge dislocations is usually considered to be

proportional to the tilted angle of the grain boundary. The tilt angle can be calculated

from Frank formula with the periodicity of edge dislocations and the Burgers vector.[32,]

[36] Consequently, the dislocation energy per unit length is related to the magnitude of the Burgers vector. The co-effect of the edge dislocations and grain boundary can produce some special transmission channel or trapping centers for carriers and influence the dielectric properties of $BaTiO_3$ nanocubes. On the other hand, these line defects and plane defects have great potential in harvesting solar energy.[37]

Fig. 9 is the schematic illustration for the crystallographic fusion behavior of $BaTiO_3$ nanocube arrangement with sintering. The semi-coherent fusion region with atom-to-atom connection of {100} crystal planes could be formed at a critical temperature. The lattice defects evolved in the connection region of nanocubes during the sintering process. The small angle grain boundaries were generated and associated with the edge dislocations. And the ions in the core of defects possessed dangling bonds. The morphology of $BaTiO_3$ nanocubes could be broken at the heat treatment of $950^{o}C$.

4. Conclusions:

In this work, a precise study on the crystallographic fusion behavior of the arrangement of $BaTiO_3$ nanocubes was carried out by using HRTEM. The nanocubes arrangement possessed a unique shape thermal stability during sintering, compared with traditional nanocrystals terminated by irregular surfaces. The regular and straight interfaces of $BaTiO_3$ nanocubes arrangements were retained even after they are sintered

at high temperature. After sintered at high temperature ($\geqq 800^{\circ}C$), the initial ambient

interface between neighboring nanocubes transformed into robust structure, and lattice

defects evolved in the region. Due to the metastable nature of lattice defects, they could

be removed by using thermal diffusion method. Well defined fusion region between

nanocubes with few of defects could be produced around $850^{\circ}C$. Combined with

previous results, the interface between nanocubes and lattice defects in the interface

region showed a critical role on the dielectric properties of the nanocube arrangements.

The systematic research on the interaction behavior of $BaTiO_3$ nanocube arrangement

can make certain contribution on the development of the application of nano-sized

perovskite materials.

Acknowledgements

Notes and references

Corresponding auther:
Phone: +81-52-736-7577
Fax: +81-52-736-7234

E-mail: qiang-ma@aist.go.jp

1   Z. Wen, C. Li, D. Wu, A. D. Li and N. B. Ming, *Nat. Mater.,* 2013, **12**, 617.

2   S. O'Brien, L. Brus and C. B. Murray, *J. Am. Chem. Soc.*, 2001, **123**, 12085.

3   R. L. Brutchey, G. Cheng, Q. Gu and D.E. Morse, *Adv. Mater.,* 2008**, 20**, 1029.

4   P. Tang, D. J. Towner, A. L. Meier, and B. W. Wessels, *Appl. Phys. Lett.,* 2004, **85**, 4615.

5   K.-H. Chen, Y.-C. Chen, Z.-S. Chen, C.-F. Yang and T.-C. Chang, *Appl. Phys. A: Mater. Sci. Process.,* 2007, **89**, 533.

6   M. Liu, C. R. Ma, G. Collins, J. Liu, C. L. Chen, C. Dai, Y. Lin, L. Shui, F. Xiang, H. Wang, J. He, J. C. Jiang, E. I. Meletis and M. W. Cole, *ACS Appl. Mater. Interfaces* 2012. **4**, 5761.

7   J. Zhou and Z. C. Yang, *CrystEngComm* 2013,**15**,8912.

8   Sasaki, T.; Endo, Y.; Nakaya, M.; Kanie, K.; Nagatomi, A.; Tanoue, K.; Nakamura, R.; Muramatsu, A. *J. Mater. Chem.,* 2010, **20**, 8153.

9   F. Dang, K. Mimura, K. Kato, H. Imai, S. Wada, H. Haneda and M. Kuwabara, *Nanoscale.*, 2012, **4**, 1344.

10 K. Kato, K. Mimura, F. Dang, H. Imai, S. Wada, M. Osada, H. Haneda and M. Kuwabara, *J. Mater., Re,* 2013, **28**, 2932.

11 K. Kato, F. Dang, K. Mimura, K. Kinemuchi, H. Imai, S. Wada, M. Osada, H. Haneda and M. Kuwabara, *Adv. Powder Technol.,* 2014, **2**5, 1401.

12 Q. Ma, K. Mimura and K. Kato, *CrystEngComm* 2014, **16**, 8398.

13 S. S. Parizi, A. Mellinger and G. Caruntu, *ACS Appl. Mater. Interfaces* 2014, **6**, 17506.

14 L. S. Gomez-Villalba, P. López-Arce, M. Alvarez de Buergo and R. Fort, *Cryst. Growth Des.*, 2012, **12**, 4844.

15 D. Yu, N. X. Xu, L. Hu, Q. L. Zhang, H. Yang, *J. Mater. Chem. C.*, 2015, **3**, 4016.

16 Z. D. Liu, Y. Feng and W. L. Li, *RSC. Adv.,* 2015, **5**, 29017.

17 Z. M. Dang, Y. Q. Lin, H. P. Xu, C. Y. Shi, S. T. Li and J. B. Bai, *Adv, Funct. Mater.*, 2008, **18**, 1509.

18 S. A. Paniagua, Y. Kim, K. Henry, R. Kumar, J. W. Perry and S. R. Marder, *ACS. Appl. Mater. Interfaces* 2014, **6**, 3477.

19 B. M. Maoz, E. Tirosh, M. B. Sadan, I. Popov, Y. Rosenberg and G. Markovich, *J. Mater. Chem.*, 2011, **21**, 9532.

20 D. V. Talapin, J. S. Lee, M. V. Kovalenko and E. V. Shevchenko, *Chem. Rev.*, 2010, **110**, 389.

21 Li, N. H.; Wu, W.; Chou, S. Y. *Nano Lett*., **2006**, *6*, 2626.

22 C. Wang, Y. J. Wei, H. Y. Jiang, S. H. Sun, *Nano Lett.*, 2010, **10**, 2121.

23 V. Gorshkov, V. Kuzmenko, V. Privman, *CrystEngComm*, 2014, 16, 10395.

24 G. M. Whitesides and B. Grzybowski, *Science* 2002, **295**, 2418.

25 L. H. Hu, C. D. Wang, R. M. Kennedy, L. D. Marks and K. R. Poeppelmeier, *Inorg. Chem.*,

2015, **54**, 740.

26 J. J. Liu, Y. C. Sui, C. G. Duan, W. N. Mei, R. W. Smith and J. R. Hardy, *Chem. Mater.*, 2006, **18**, 3878.

27 X.-H. Wang, X. -Y. Deng, H. L. Bai, H. Zhou, W. G. Qu, L.-T. Li and I.-W. Chen, *J. Am. Ceram. Soc.*, 2006, **89**, 438.

28 D. Hull, and D. J. Bacon, *Introduction to Dislocations*, *4th ed.*; Oxford: Oxford, 2001, Vol. Butterworth-Heinemann.

29 D. M. Tang, C. L. Ren, M. S. Wang, X. L. Wei, N. Kawamoto, C. Liu, Y. Bando, M. Mitome, N. Fukata and D. Golberg, *Nano Lett.*, 2012, **12**, 1898.

30 M. I. Bodnarchuk, E. V. Shevchenko and D. V. Talapin, *J. Am. Chem. Soc.*, 2011, **133**, 20837.

31 Z. C. Wang, M. Saito, K. P. McKenna and Y. Ikuhara, *Nat. comms.*, 2014, **5**, 3239.

32 A. Nakamura, T. Mizoguchi, K. Matsunaga, T. Yamamoto, N. Shibata and Y. Ikuhara, *ACS NANO* 2013, **7**, 6297.

33 Z. J. Shen, H. X. Yan, D. Grüner, L. M. Belova, Y. Sakamoto, J. F. Hu, C. W. Nan, T. Höche and M. J. Reece, *J. Mater. Chem.*, 2012, **22**, 23547.

34 B. Nikoobakht, J. Bonevich and A. Herzing, *J. Phys. Chem. C.,* 2011, **115**, 9961.

35 R. L. Penn and J. F. Banfield, *Science* 1998, **281**, 969.

36 F. C. Frank, *Crystal Dislocations.-Elementary Concepts and Definitions*. *Philos. Mag.*, 1951, Vol. **42**, pp 809-819.

37 Z. K. Zheng, W. Xie, Z. S. Lim, L. You and J. L. Wang, *Sci. Rep.,* 2014, **4**, 5721.

Fig. 1 FE-SEM images of BaTiO$_3$ nanocubes arrangements (a) without sintering; (b) with sintering at 800°C; (c) with sintering at 850°C; (d) with sintering at 900°C for 1 hour under oxygen gas atmosphere.

Fig. 2 The TEM image of two neighboring BaTiO$_3$ nanocubes without sintering.

Fig. 3 TEM images of BaTiO$_3$ nanocubes arrangement with sintering at (a) 800°C; (b) 850°C; (c) 900°C and (d) 950°C for 1 hour under oxygen gas atmosphere.

Fig. 4 (a) High resolution TEM image and (b) its corresponding FFT filtered image of quarto point region of four BaTiO$_3$ nanocubes arrangement with sintering at 800°C for 1 hour under oxygen gas atmosphere.

Fig. 5 (a) High resolution TEM image and (b) its corresponding FFT filtered image of quarto point region of four BaTiO$_3$ nanocubes arrangement with sintering at 850°C for 1 hour under oxygen gas atmosphere.

Fig. 6 (a) High resolution TEM image, and (b) its corresponding FFT filtered image of irregular triple point region of three BaTiO$_3$ nanocubes arrangement with sintering at 900°C for 1 hour under oxygen gas atmosphere.

Fig. 7 (a) High resolution TEM image, and (b) its corresponding FFT filtered images of interface region of two BaTiO$_3$ nanocubes arrangement with sintering at 950°C for 1 hour under oxygen gas atmosphere; (c) the FFT filtered image of Figure 7 (a) by using only one set of [100] spots.

Fig. 8 (a) and (c) High resolution TEM images; (b) and (d) their corresponding FFT filtered images of two kinds of sintered BaTiO$_3$ nanocubes arrangements with small angle grain boundary.

Fig. 9 Illustration for the crystallographic fusion behavior of BaTiO$_3$ nanocube arrangement with sintering
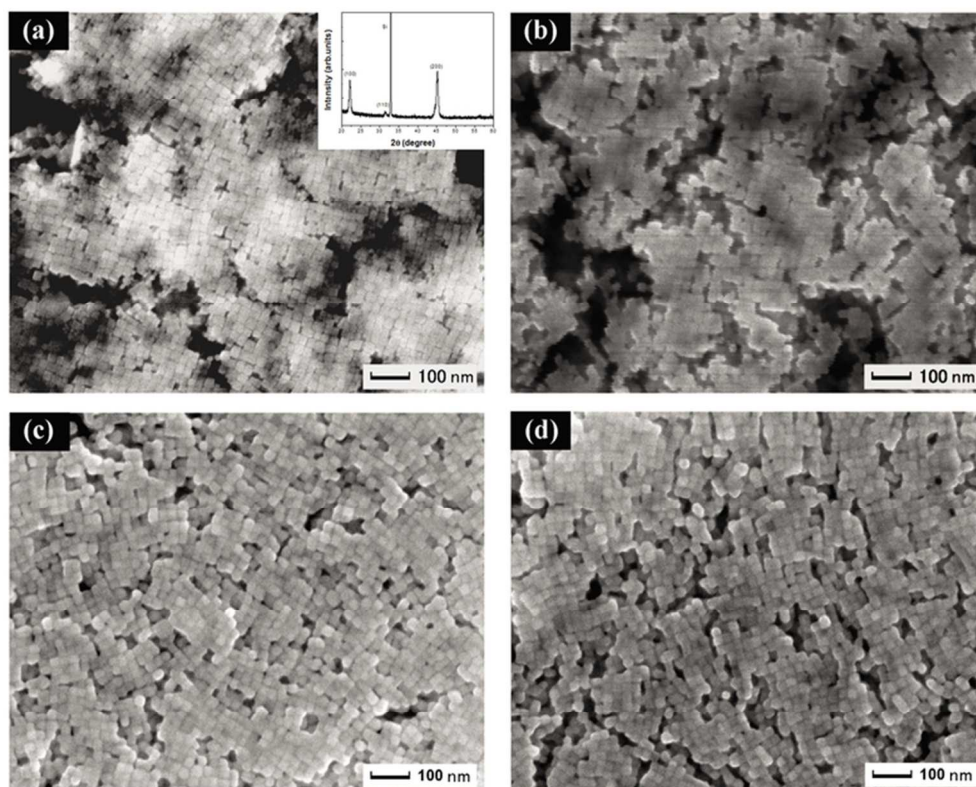
67x55mm (300 x 300 DPI)
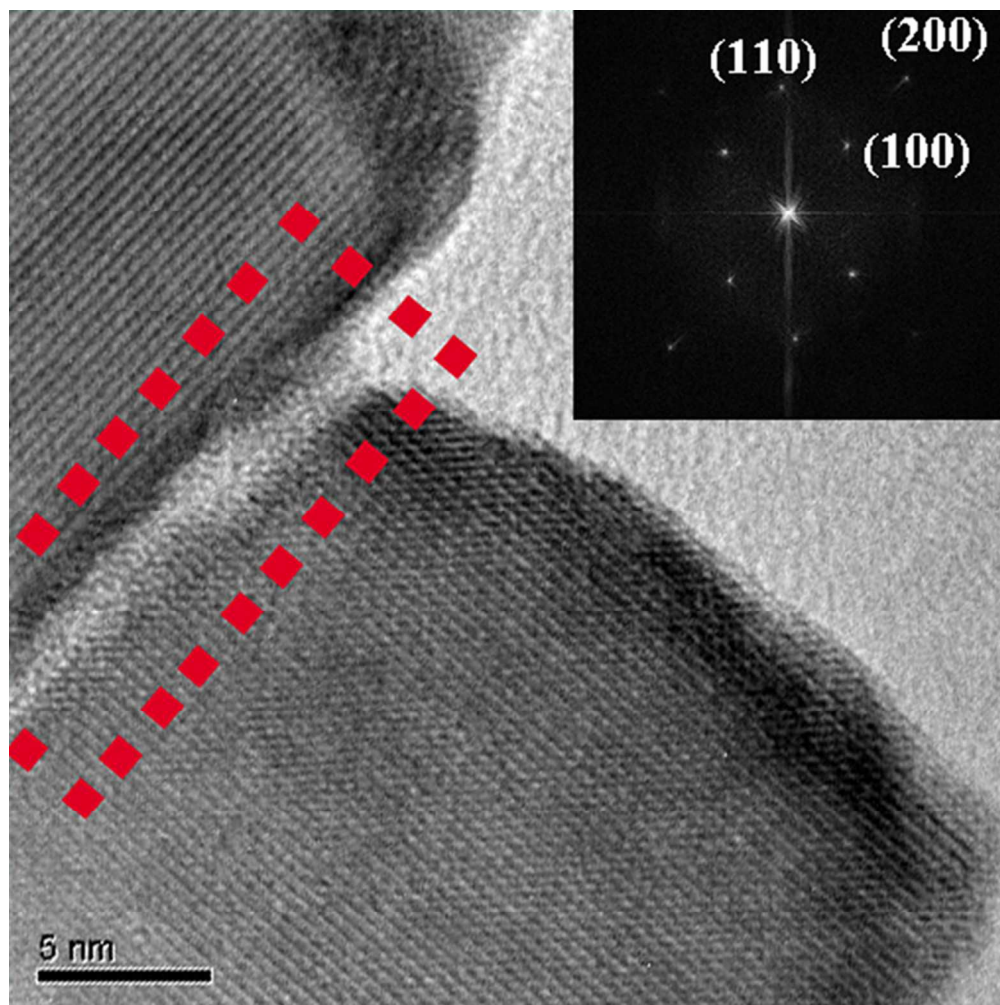
135x135mm (150 x 150 DPI)
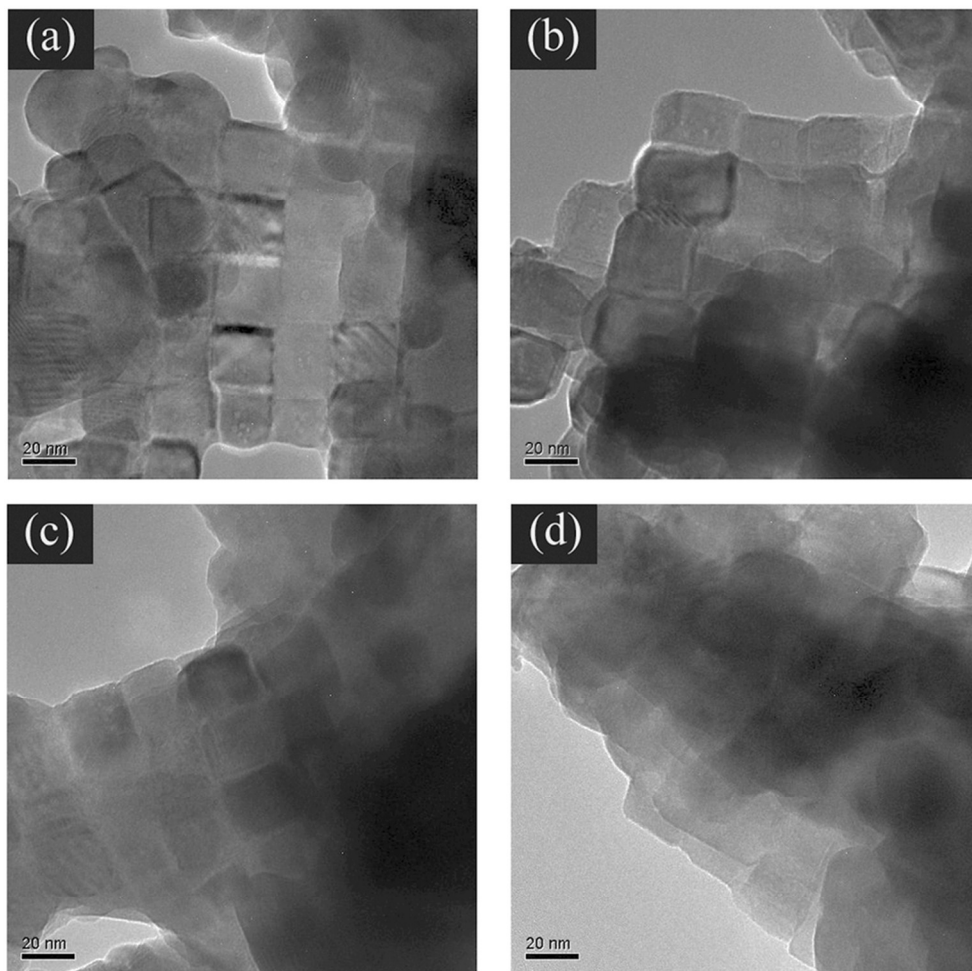
82x82mm (300 x 300 DPI)
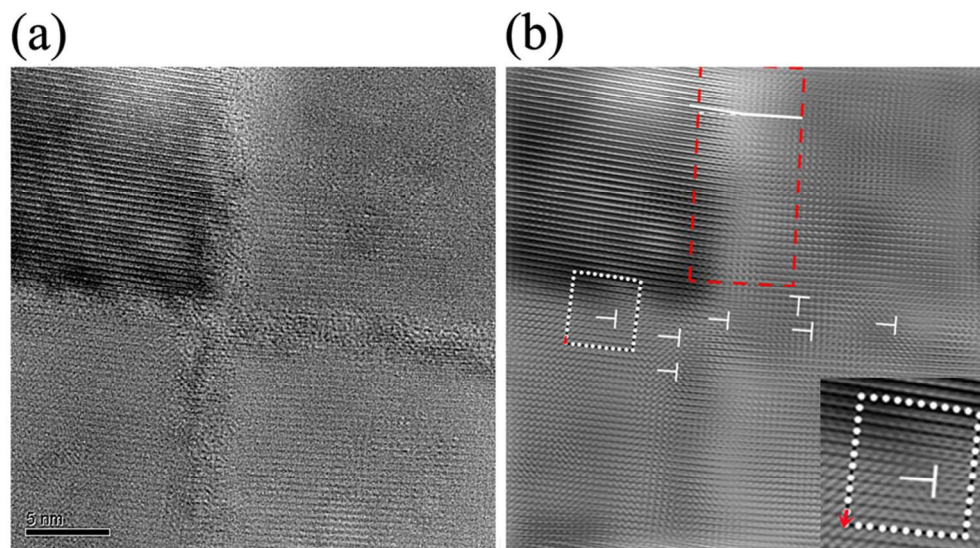
89x51mm (300 x 300 DPI)
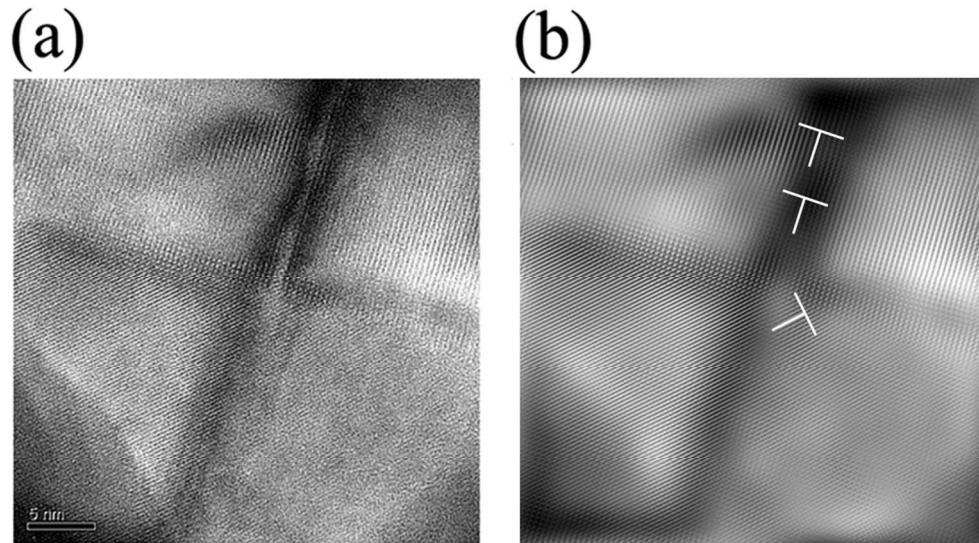
101x55mm (300 x 300 DPI)
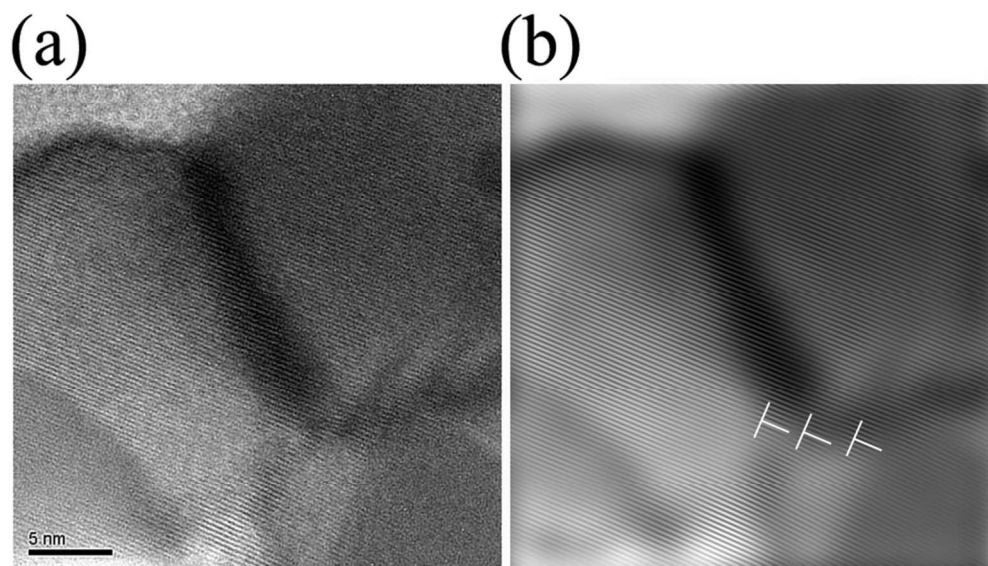
88x50mm (300 x 300 DPI)

93x101mm (300 x 300 DPI)
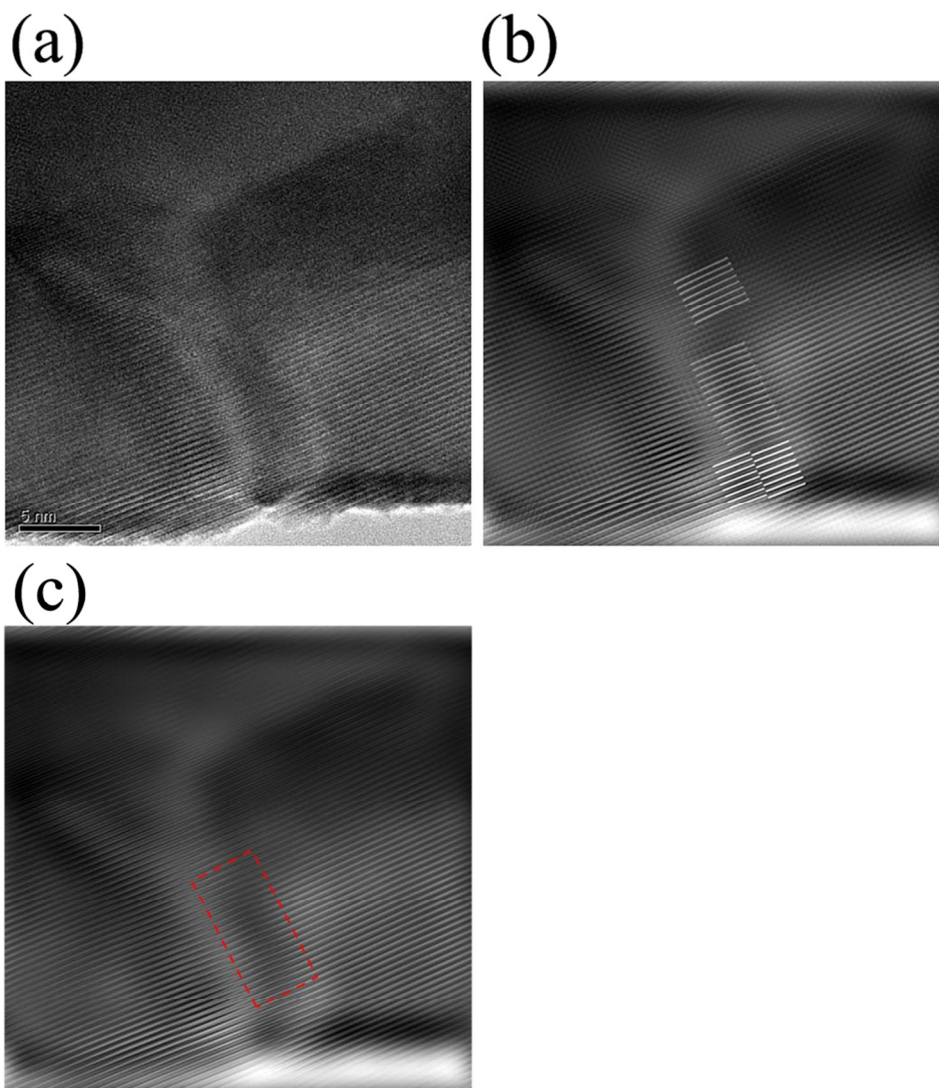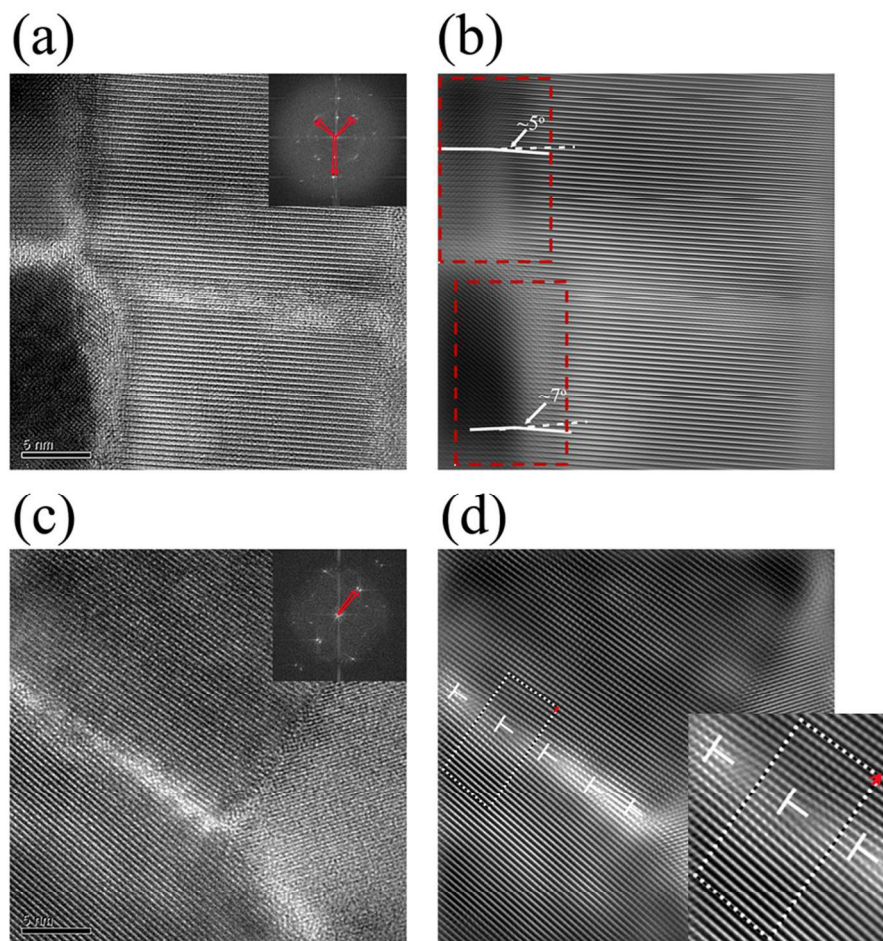
194x193mm (300 x 300 DPI)
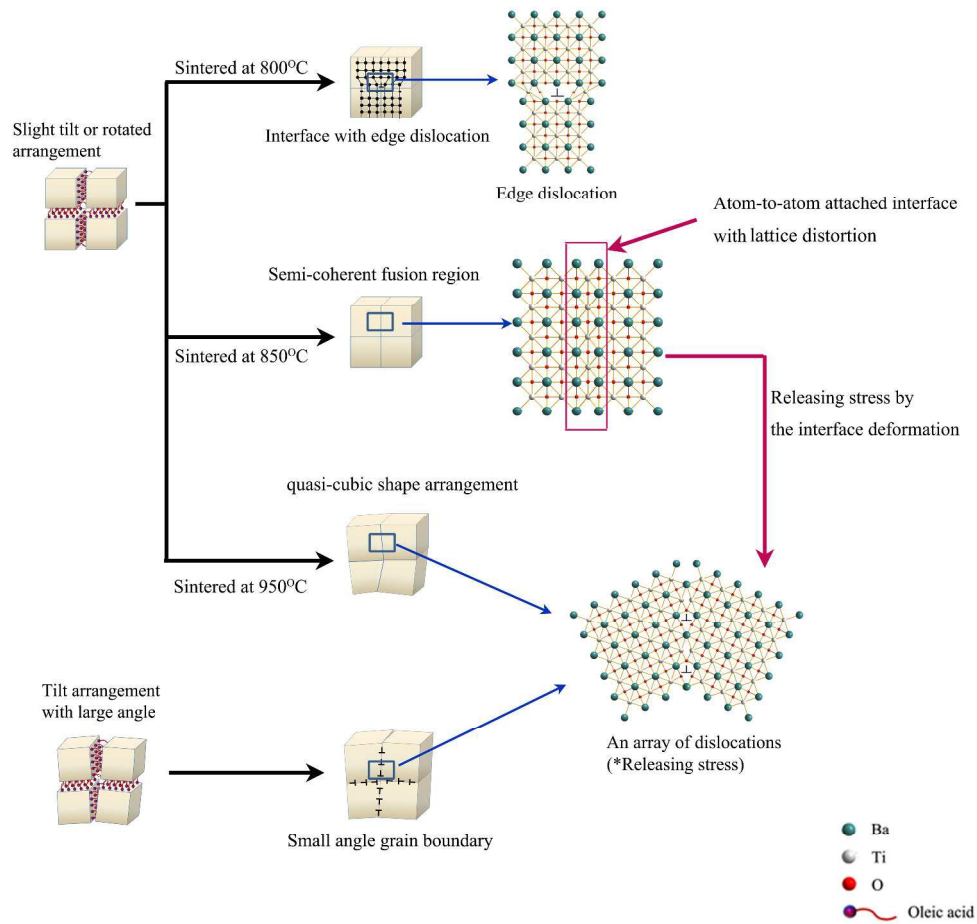
Fig. 9 Illustration for the crystallographic fusion behavior of BaTiO$_3$ nanocube arrangement with sintering
399x381mm (300 x 300 DPI)
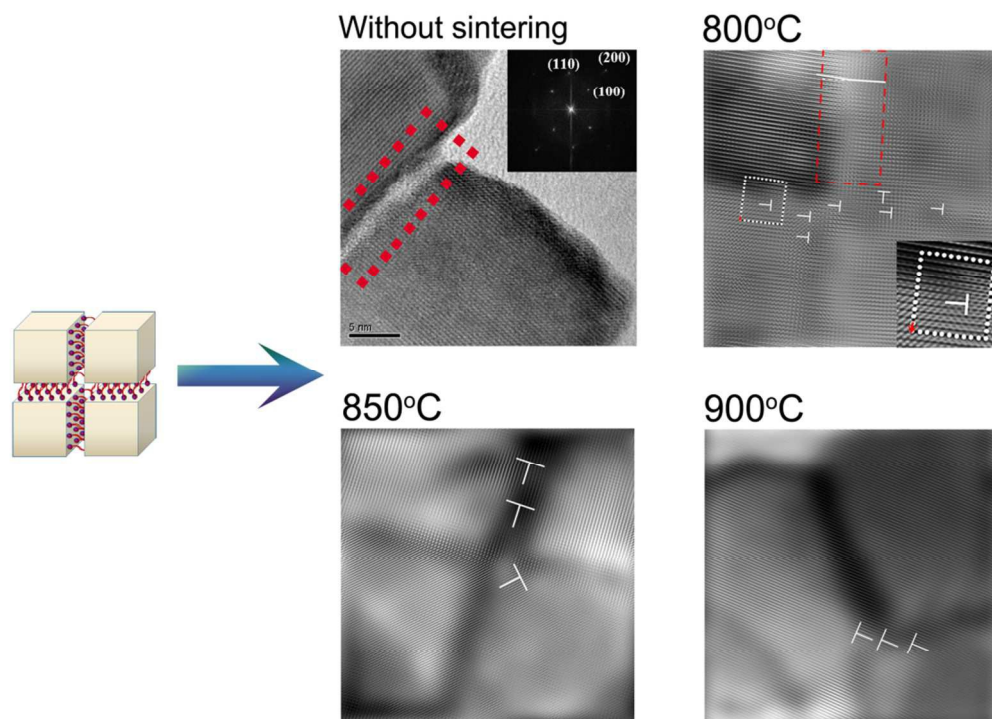
An abnormal sintering behavior between $BaTiO_3$ nanocubes with variable sintering temperatures and geometries was investigated by precise analysis using high resolution transmission electron microscopy (HRTEM). The fine orderly microstructure of nanocubes arrangement remained even after high temperature sintering process ($\sim$900°C), where the face-to-face connection with simple cubic symmetry was stable. In the case of the small angle relation of nanocubes, the initial ambient interface changed into robust structure at one critical sintering temperature, and the finally lattice defects evolved in the interface region. The lattice fringes in different nanocubes grew and connected via an atom-by-atom epitaxial attachment mechanism around 850°C. The amount of defects has a close relationship with the sintering temperature.